Spreading of thin-film metal patterns deposited on nonplanar surfaces using a shadow mask micromachined in Si (110)

R. M. Tiggelaar
Mesoscale Chemical Systems Group, and Transducers, Science and Technology Group, MESA+ Institute for Nanotechnology, University of Twente, P.O. Box 217, 7500 AE Enschede, The Netherlands

J. W. Berenschot and M. C. Elwenspoek
Transducers, Science and Technology Group, MESA+ Institute for Nanotechnology, University of Twente, P.O. Box 217, 7500 AE Enschede, The Netherlands

J. G. E. Gardeniers[a)]
Mesoscale Chemical Systems Group, MESA+ Institute for Nanotechnology, University of Twente, P.O. Box 217, 7500 AE Enschede, The Netherlands

R. Dorsman and C. R. Kleijn
Department of Multiscale Physics, Delft University of Technology, Prins Bernhardlaan 6, 2628 BW, Delft, The Netherlands

(Received 15 March 2007; accepted 15 May 2007; published 25 June 2007)

The application of a three dimensional, self-aligning shadow mask in (110)-oriented silicon for thin-film metal deposition is discussed. This shadow mask is used for the deposition of metal tracks on the bottom of structures with vertical sidewalls, i.e., the patterning of metal catalytic patches underneath the membrane that covers the deep flow channel of a high-temperature gas microreactor. The accuracy of this patch definition—pattern spreading—is investigated for rhodium and platinum as a function of the mask-to-substrate distance. The pattern of sputter-deposited patches is subject to pattern spreading when the gap between the shadow mask and the substrate is nonzero. The experimental patch widening shows a square root dependency on the gap size. Via numerical simulations of molecular gas flows using a direct simulation Monte Carlo method, it is shown that there is excellent agreement between the observed experimental data and this model taking into account values for the sticking (γ) and accommodation (α) coefficients of the atoms on the walls of the shadow mask below unity (i.e., $\gamma=0.5$ and $\alpha=0.1$), and a baseline shift due to curvature and/or bending of the shadow mask and/or substrate. © *2007 American Vacuum Society.*
[DOI: 10.1116/1.2747629]

I. INTRODUCTION

An important trend in microelectromechanical systems (MEMS) is the development of increasingly complex three-dimensional (3D) microstructures with integrated functionality. In particular, the integration of sensor and actuator elements on surfaces with high aspect ratio microstructures has become of interest, but developments have been limited due to the difficulties that arise in photolithography on such surfaces. Important parameters that determine the quality of feature definition are the distance between mask and resist surface and thickness and uniformity of the photoresist layer. These parameters are difficult to control if surface topography of tens to hundreds of microns is present on the substrate surface, which is not uncommon in MEMS fabrication.[1–3] Spin or dip coating on nonplanar surfaces gives rise to photoresist thickness variations at corners of structures due to capillary effects and reflow, and even if relatively thick resists of 20 μm or more are used to planarize the surface,[4] pattern resolution will be nonuniform and generally not adequate for further processing. Spray coating[5,6] is much better in this respect, but also cannot completely overcome thickness variations at corners of high aspect ratio microstructures. The best way to achieve conformal deposition over surface topography is to use electrodeposition of special photoresists.[7–9] With this method, electroplated Ni cantilevers and coils with a linewidth of 25 μm were fabricated on 54.7° inclined sidewalls of 300 μm deep cavities in silicon.[10,11] As an alternative to this, Kutchoukov *et al.* developed a two-step spin coating procedure for conformal coating on (100) silicon with KOH etched through holes and cavities.[4,12] Conformality could be further improved by smoothening of convex silicon corners with a short tetra methyl ammonium hydroxide (TMAH)-etch step. Copper tracks of 20 μm width were realized with lift-off in 525 μm deep through holes. This work demonstrated that with a resist coating of good uniformity, pattern definition on substrates with topography is limited only by Fresnel diffraction, which occurs due to the nonzero gap between mask and substrate and thus becomes more important at the deeper parts of a recessed area.

Photoresist processing may not be the best option for patterning thin-film patterns on fragile microstructures such as membranes with a thickness below 5 μm, since spin coating

a)Author to whom correspondence should be addressed; electronic mail: j.g.e.gardeniers@utwente.nl

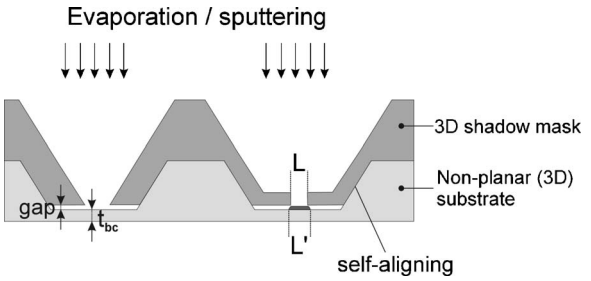

FIG. 1. Illustration of material deposition on topographically patterned substrates (nonplanar surfaces) using a "self-aligning" 3D shadow mask—*gap* is the gap between the shadow mask and the substrate, t_{bc} is the thickness of the bottom of the cavity on which a pattern will be deposited, L is the length of the mask opening and L' is the length of the pattern deposited.

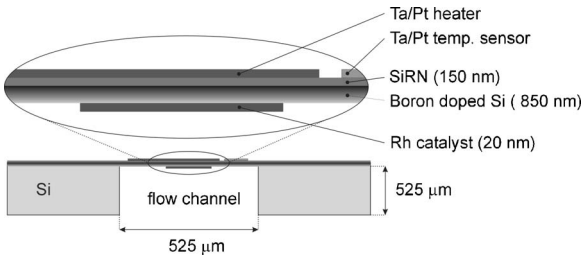

FIG. 2. Cross section of flow channel and membrane with heater and catalyst patterns (top wafer only; channel closed with Pyrex wafer containing powder blasted access holes for gasses).

and particularly ultrasonic lift-off procedures give rise to unacceptable stress and vibrational resonance of the microstructure, frequently resulting in rupture.

To overcome the difficulties with photoresist processing, we investigated shadow masking as an alternative manner of pattern generation. This relatively old method is consisted in the deposition of a material through holes cut in, for example, a metal foil by laser or other means. Micromachined silicon shadow masks have been used to deposit patterns with dimensions down to several tens of microns on flat surfaces.[13] With the aid of piezoactuators to establish controlled and precise movement of a shadow mask in six directions, an alignment accuracy of approximately 1 μm has been achieved.[14] If silicon micromachining techniques are combined with focused ion beam (FIB), laser-interference lithography, or electron beam lithography, submicron features become possible.[15,16] For example, stencil masks based on silicon nitride membranes suspended in silicon frames and partially opened using e-beam lithography in combination with reactive ion etching or FIB milling were used to deposit patterns with a size down to 100,[17,18] 50,[19–22] and even down to 20 nm with molecular beams,[23] and arrays of dots in the range of 15–35 nm.[24–27]

The examples above concerned the deposition on flat surfaces. If shadow masks were used to deposit patterns on surface with topography, it was found possible to evaporate metal wires of 10 μm with a pattern resolution of 3 μm in and across 380 μm deep KOH-etched cavities, resulting in an electrical wafer feedthrough.[28] However, spreading, in the form of a smooth decay at the edges of evaporated material underneath shadowed parts, was observed, which increased for higher evaporation rates and smaller mask apertures. This spreading was attributed to a combination of two effects: (i) the vapor source is not a real point source, which results in a penumbra region at pattern edges; and (ii) due to a sticking coefficient less than 1, atoms will scatter at mask edges or substrate, resulting in material deposition in shadowed areas.[29]

To reduce the spreading problem, a shadow mask can be used, that is a negative replica of the topography of the device wafer, see Fig. 1. Besides the fact that in this way the distance between mask and substrate at the position of interest is minimized, the mask may also be modified such that it self-aligns in recessed areas. For best resolution, the gap should be zero (i.e., mask and substrate are in direct contact); however, if deposition is planned on a fragile membrane, nonzero gaps are recommendable. Brugger *et al.*[30] used a shadow mask fabricated out of (100) Si with KOH etching for evaporation of 10×50 μm^2 rectangles on the bottom of 500 μm deep cavities. Due to the small gap between mask windows and the substrate, little spreading of the patterns was measured. The self-aligning feature on 54.7° sloped {111} planes was also used to evaporate 25 μm wide aluminum wires across a 120 μm high step with no change in dimensions between top, sidewall, and bottom. Similarly, a micromachined shadow mask was used to deposit well-defined catalyst patches on a membrane with, on the other side, a thermoelectric generator functioning through catalytic combustion reactions.[31]

Stimulated by this latter work, we have conducted a study on the characteristics of the deposition of such catalyst patches in deep rectangular trenches in silicon. These trenches serve as the flow channel of a microreactor designed for catalytic partial oxidation (CPO) reactions. To have a well-defined system for a kinetic study of these reactions and in order to prevent formation of secondary products, deposition of catalyst on the sidewalls of the flow channel had to be avoided. The catalytic material (e.g., rhodium, used for direct CPO of methane into synthesis gas[32,33]) should be deposited only on the central area of the membrane, where a heater resistor pattern was deposited on the outside of the membrane. The area and thickness of the catalyst layer should also be well defined. A cross section of the microreactor is shown in Fig. 2. Details about the fabrication and the performance of the microreactor can be found elsewhere.[34,35] The membrane consisted of a layer of 850 nm of heavily boron-doped silicon covered by a layer of 150 nm of silicon nitride, which gives a structure with excellent thermomechanical properties, but which is too fragile to withstand the resist spinning process for photolithography. Therefore, patternings of the catalyst on the channel side of the membrane and heaters and temperature sensors on the outside of the membrane were performed with shadow mask processes. The topic of this article is to investigate the accuracy of catalyst patch definition, i.e., the pattern width as a function of the mask-to-substrate distance.

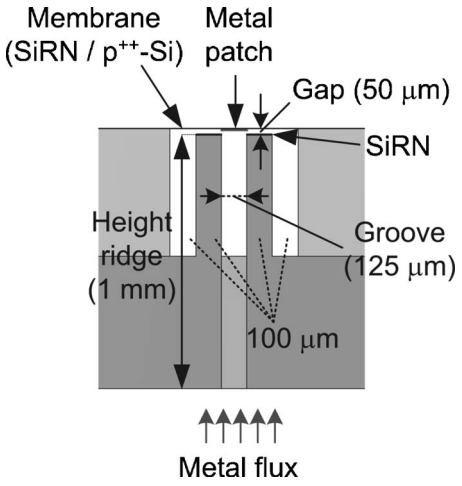

FIG. 3. Self-aligning shadow mask etched in (110)-Si substrate, positioned in a deep flow channel to deposit, e.g., a metal catalyst.

II. EXPERIMENT

For shadow mask manufacture it was decided to use KOH etching in {110}-oriented silicon, which allows the fabrication of narrow grooves bound by vertical Si {111} planes, with a depth-to-width ratio of up to 100:1.[36] The process was also used to create alignment ridges which can be lowered into the described microreactor flow channel. Between the alignment ridges a slit was created through which a metal was sputtered onto the bottom side of the membrane, as shown in Fig. 3.

The shadow mask was designed such that the length of the ridges is almost identical to the length of the flow channel (30 mm) to obtain self-alignment in the length direction of the channel. The gap between the ridges and the membrane can be tuned by exact timing of the KOH etching process.

Fabrication of the shadow mask was performed on a 1 mm thick (110)-oriented silicon wafer, in a 25 wt % KOH solution at 75 °C. This wafer thickness was selected for stability and handling purposes during fabrication and deposition. The fabrication procedure is shown in Fig. 4. First, a layer of 200 nm low stress silicon-rich silicon nitride[37] (SiRN) is deposited on a (110)-silicon wafer by low pressure chemical vapor deposition, and the exact crystallographic orientation of the wafer is determined using an alignment mask[38] (this step is not shown in Fig. 4). Next, in the SiRN layer at the top side of the wafer the desired pattern is preetched using lithography and reactive ion etching (RIE), see step B in Fig. 4. Two openings of 120 μm $\times$ 4.1 mm, used to define catalyst patches, and several resolution test patterns are defined, and the SiRN layer is locally reduced to 50 nm, which is acting as a KOH mask (the reduced pattern is a "hidden mask"—see step E). Then the shadow mask slit is opened from the back side of the wafer, using standard lithography and KOH etching (step C). After etching the slit to a depth of about 500 μm, the alignment ridges are defined at the top side of the wafer using standard lithography and plasma etching of the SiRN. In the second KOH-etch step the slit is completely etched through the wafer (slit width of approximately 125 μm after KOH etching), while in the same etching process the alignment ridges are created (step D). The last step consists of opening the previously defined catalyst patches and test patterns (the hidden mask mentioned above) in the SiRN layer by RIE (step E). Figure 4 also shows a top view of the windows in the SiRN layer between the alignment ridges. The small test patterns consisting of circles and squares are used to study the dimensional resolution of the metal deposition.

Sputter deposition of different metals was performed on a home-built sputter machine with three 2 in. dc magnetron guns. During sputtering, the substrate holder was rotated at a frequency of about 0.5 Hz. For a comprehensive study of pattern spreading, the metals rhodium (Rh) and platinum (Pt) were sputtered, either through the shadow mask described above or without mask, on flat substrates, with argon as the

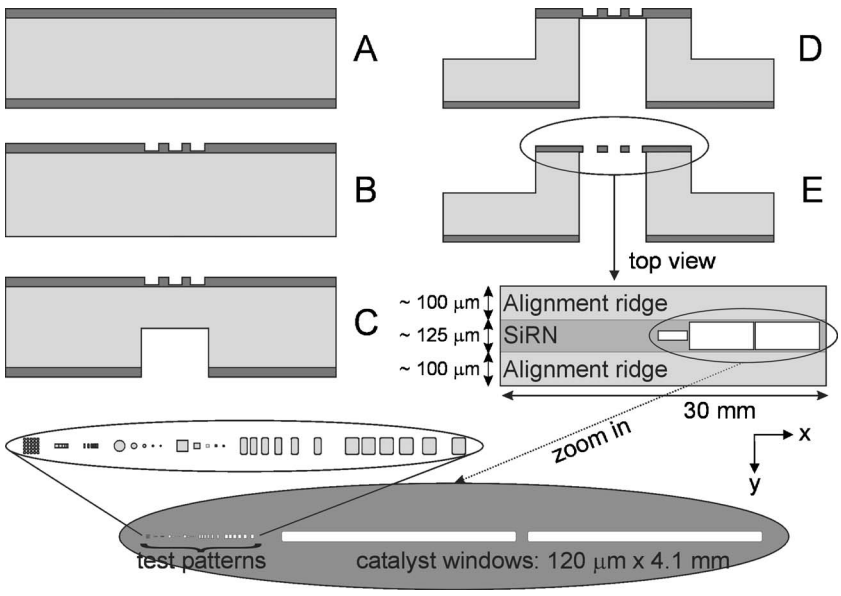

FIG. 4. Fabrication scheme of self-aligning shadow mask in (110) Si (not on scale; dimension test patterns given in Fig. 6 and Sec. III).

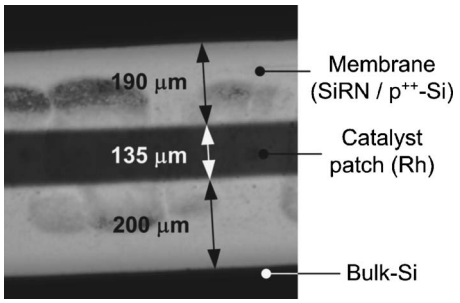

FIG. 5. Optical microscope picture of a rhodium catalyst patch viewed through the thin capping membrane of the microreactor; the width of the catalyst windows in the shadow mask is 120 μm.

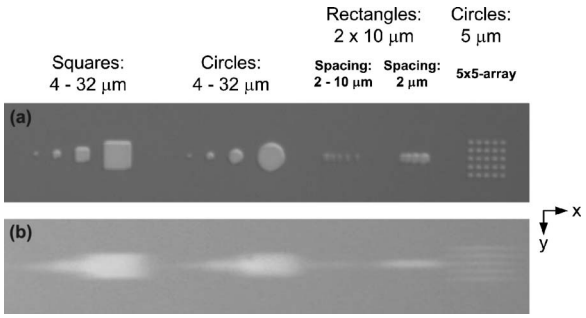

FIG. 6. Pictures of test patterns of rhodium when the gap between mask and substrate is ~0 μm (a) and ~25 μm (b) (the alignment ridges of the shadow mask were directed in the x direction; $P \sim 200$ W).

working gas. In all sputtering experiments the system was pumped down to a pressure below 3×10^{-6} mbar. Just before a sputter run, the targets of interest were sputter cleaned for 2 min. All sputtering runs were performed for 15 min at an argon pressure of $(6.6 \pm 0.1) \times 10^{-3}$ mbar (0.67 Pa) with the substrate kept at room temperature. The input power to the target was fixed to 200 W. Both targets were of 99.95% purity or better.

The thickness of deposited metal films was measured with a Veeco Dektak8 step profiler. The measured thicknesses, and hence deposition rates, of metal layers deposited through the shadow mask were compared with the deposition rate on flat surfaces without shadow mask. For the layer thickness on flat surfaces the scan length was 1 mm (scan time: 30 s, scan force: 5 mg); measurements were repeated three times at different positions on the substrate. For the patterns deposited through the shadow mask windows the scan length was 500 μm (identical scan time and force) and the measurements were repeated five times. After each profile measurement, a zoom in on the data was performed and subsequently this raw data was levelled such that in the profile a transition zone (i.e. a "step" in the height) was clearly observed. For nonzero gaps between shadow mask and the substrate, spreading of the deposited patterns occurs. For a variety of gaps this spreading was determined with an optical microscope and a charge coupled device (CCD) camera.

III. RESULTS

In a first experiment, sputter deposition of rhodium was performed in the flow channel of the microreactor, using the described self-aligning shadow mask. Figure 5 shows a typical result for a Rh catalyst track, viewed through the capping membrane of the microreactor. It can be seen that the rhodium patch was misaligned approximately 5 μm with respect to the center of the membrane, which is mainly due to manual lowering of the 3D-shadow mask in the flow channel of the microreactor. No deposit was found on the sidewalls of the flow channel. The pattern width is 135 μm, compared to the 120 μm width of the mask window. This spreading is due to a small but nonzero gap of approximately 25–35 μm between mask ridges and membrane. The height of the ridges was about 500 μm, whereas the channel was 525 μm deep. The thickness of the Rh patches was 20 ± 5 nm, which was about a factor of 10 lower than the thickness measured on a flat uncovered substrate.

In a second series of experiments the profile of the patterns deposited through the shadow mask was studied. As was already clear from Fig. 5, the patterns become spread out if the gap between mask and membrane is not zero. To study this effect, gaps of 0, 25, and 150 μm between the shadow mask and a flat substrate surface were created, using spacers. The gap accuracy in all cases was approximately 15 μm, due to small variations in substrate and/or spacer thickness, as well as a slight curvature of the substrate on which the metal was sputtered. Figure 6 shows the result of Rh deposition through circular and rectangular windows with sizes up to 32 μm in length and width, for gaps of 0 and 25 μm. In the latter case spreading can clearly be identified from the blurring of the patterns. A remarkable result is that pattern spreading is not symmetrical, it is much larger in the x direction (horizontal direction in Fig. 6) than in the y direction. Figure 7 shows thickness profiles of a Rh deposit through an opening with a size of $L_y = 120$ μm and $L_x = 4.1$ mm for a shadow mask-substrate gap of 25 μm. This figure demonstrates that the spreading in the x direction is a factor of 3–4 larger than that in the y direction.

For mask-to-substrate gaps up to 150 μm, the spreading in the deposited patterns was measured with an optical microscope (Olympus) using polarized light, a CCD camera, and a computer. Measurements on the deposited patterns were repeated five times. Since for gaps above 25 μm pattern spreading in the x direction was larger than the designed distance between the test structures, accurate determination of spreading in this direction was not possible. The thickness measurement in the x direction in Fig. 7 was performed on the catalyst structures. Therefore, for a quantitative evaluation only the pattern enlargement in the y direction will be considered. In detail, for gaps of 25 μm and larger only data for catalyst windows with $L_y = 120$ μm and $L_x = 4.1$ mm and test patterns with $L_y = 50$ μm and $L_x = 40$ or 20 μm were found to be useful; smaller structures were blurred and ill defined (as shown in Fig. 6).

In Fig. 8 the spreading of four different structures (two with the same size but at different locations on the mask) of Rh and Pt is shown as a function of the gap between mask

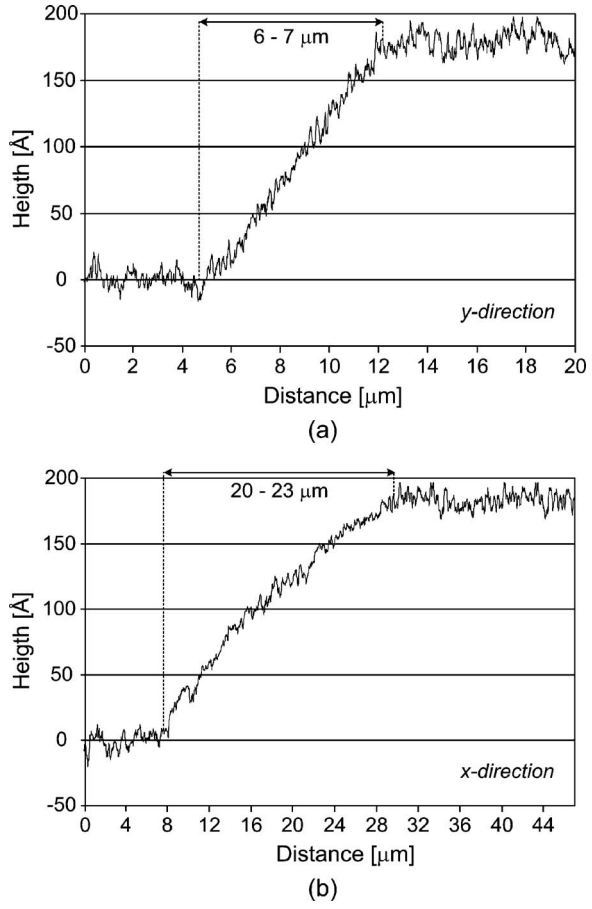

FIG. 7. Thickness profiles of sputtered rhodium patterns (window opening L_y=120 μm$\times L_x$=4.1 mm) when the gap is ~25 μm: profile perpendicular to alignment ridges of the mask (y direction) (a) and profile parallel to these ridges (x direction) (b).

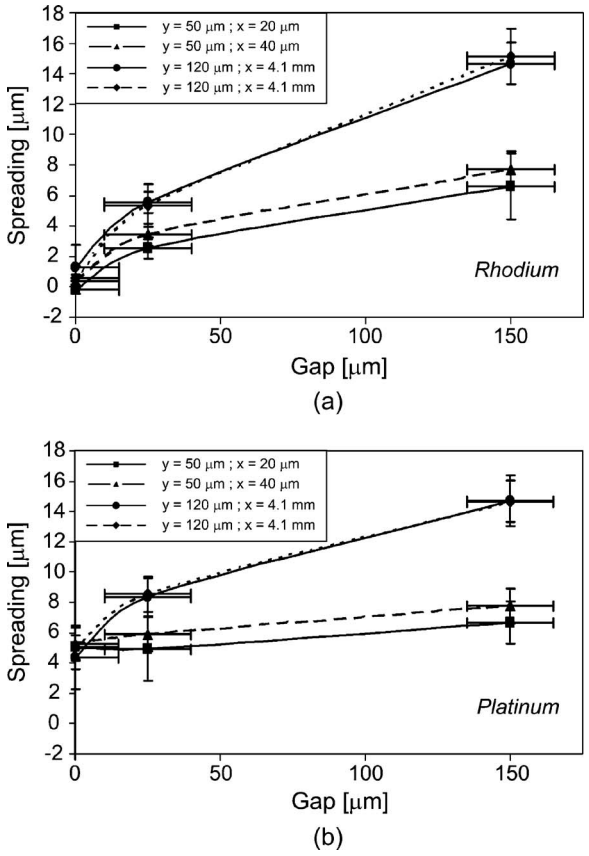

FIG. 8. Spreading of sputtered patterns of rhodium (a) and platinum (b) as a function of the gap between the substrate and the alignment ridges of the mask; spreading determined in the y direction with an optical microscope (size of window openings in the y and x directions shown in legend).

and substrate. The spreading is defined as the total width of the sputtered metal pattern minus the width of the window in the shadow mask, divided by 2 to get the pattern enlargement on one side. Clearly, for both metals the spreading of the deposited structures increases with increasing gap, the data points suggest a square root dependence. Moreover, the spreading increases almost linearly with the width of the window in the y direction, whereas the change in spreading due to a change in the width in the x direction seems negligible. The latter was expected because of the large length-to-width ratio of the trench in the shadow mask (30 mm vs 125 μm). As a consequence, a two-dimensional (2D) model can be used to investigate the patterns of the structures sputtered through the shadow mask (see Sec. IV). Finally, no significant difference in spreading between the two metals is observed; it is noted that in case of platinum the gap was not 0 μm during deposition [Fig. 8(b)].

IV. DISCUSSION

In order to be able to understand the observations, it is important to establish the transport properties of the atoms when they reach the trench between the alignment ridges. The degree of thermalization of sputtered atoms is an important parameter in the theoretical description of sputter rates. Thermalization is the process by which atoms that are sputtered from a target that is bombarded by high-energy ions (here Ar^+) slowly lose their initial high kinetic energy due to collisions with the gas atoms while they move away from the target. Eventually the sputtered atoms will reach a temperature close to or somewhat above ambient, i.e., room temperature. It was found experimentally that thermalized atoms finally reached a steady-state temperature of approximately 350 K.[39] The fact that in most cases the atoms do not cool down completely to ambient temperature is due to the inability of the gas to lose kinetic energy to the environment, because at the pressures at hand, the number of collisions with the walls of the system is negligible. Thermalization depends on pressure, the kinetic energy of the atoms, which is not constant in time due to collisions and shows an energy distribution with a high peak at about half the binding energy of the solid metal and a long tail stretching to the energy of the incident ions,[40] and on the distance that the atoms have traveled. Normally, in a magnetron sputtering system, which operates at relatively low pressures, a large fraction of the sputtered atom flux will arrive at the substrate surface with kinetic energies considerably higher than the energy they would have at ambient temperature.[40] For the used experimental conditions, with a pressure of 6.6×10^{-3} mbar, a

TABLE I. Maximum spreading in the y direction for simple line-of-sight model without interatom and sidewall collisions.

Gap between shadow mask and substrate (μm)	Spreading for window-opening of 50 μm (in the y direction) (μm)	Spreading for window-opening of 120 μm (in the y direction) (μm)
25	2.2	3.1
150	13.1	18.4

substrate-to-target distance of ~18.5 cm and Ar^+ energies of 360–600 eV, it can be estimated that the average kinetic energy of the sputtered atoms at the position of the target is approximately 0.2 eV, with some minor variations in this value depending on the mass of the sputtered atoms.[40–42] From the article by Westwood,[41] it can be derived that in this case the mean free path between collisions is in the range of 7–10 mm, which means that atoms have undergone more than 20 collisions before reaching the shadow mask. Therefore, since after every collision the direction of movement of the atoms has changed over an angle of between 10° (for the heavier atoms) and 40° (for the lighter atoms), at the position of the trench entrance hardly any angular preference of atomic movement can be expected.

In the following we will concentrate on the transport *inside the trench*. The dimensions of the 1 mm deep trench are such that its width in the y direction, 125 μm, is smaller than the mean free path of the atoms in the gas. This implies that atoms that enter the trench will collide more with the sidewalls of the trench than with other atoms. The width in the x direction, 30 mm, is a few times larger than the mean free path, so that particles might in principle collide a few times with other atoms before reaching the substrate (at the bottom of the trench). However, due to the fact that after each collision the direction of movement changes randomly over at least 10°, most of these particles would still hit the sidewalls of the trench. Now, if we assume that atoms which hit a wall will stick to that wall with unit probability ($\gamma=1$), only those atoms that have traveled from the top opening to the substrate directly will lead to growth of the metal pattern. This so called line-of-sight model leads to maximum spreading values shown in Table I. Comparison of these values with the measured values in Fig. 8 shows that for a small gap the measured values are higher than the calculated ones, while for a large gap the measured values are significantly lower. Moreover, for a line-of-sight model with $\gamma=1$, the pattern spreading increases linearly with the gap size (and values for the spreading depend on the geometry and dimensions of the mask openings), which is clearly not the case for the experimental data (Fig. 8). Thus it can be concluded that this simple line-of-sight model cannot be used to describe the spreading in the deposited patches.

A (slightly) increased temperature of a surface (i.e., the mask and/or membrane) can result in γ values smaller than unity. Several groups have studied the energy flux to the substrate during (magnetron) sputtering, and it was found that a variety of processes contribute to this flux,[39,43–46] such as the condensation heat of the film material, the kinetic energy of the sputtered atoms, plasma radiation, ion neutralization and reflection at the target, and electron impact on the substrate surface. The main conclusion was, however, that "even the accurate calculation of all heat fluxes towards a substrate does not guarantee the real evolution of the thermal condition at the substrate."[47] Thus, it is reasonable to assume that for sputtering processes γ can be smaller than unity, but it is impossible to calculate exact values. Another argument for γ values smaller than unity is that the sidewalls of the trench as well as the membrane are smooth and clean (outgassed).

Since analytical solutions for line-of-sight models with $\gamma<1$ are complicated and difficult, the experimental results are compared to numerical simulations to find an explanation for the observed patch spreading. The method that is applied is based on the direct simulation Monte Carlo (DSMC) method.[48] This method calculates flow and transport in gases by tracing the paths of individual atoms, including their collisions with each other and with any surfaces in the domain. Since the mean free path of atoms ranges from 7 to 10 mm, intermolecular collisions inside the trench are relatively infrequent. Therefore, the DSMC method is almost reduced to a ray tracing method, using straight atomic paths from one surface interaction to the next. However, even though interatomic collisions are very infrequent, and have only a very small influence on the final results, they are included in the simulations due to the fact that a standard DSMC code[49–51] was used. The DSMC method allows for a wide range of physical parameters and properties to be included in the interaction of an atom with a surface. The main surface properties relevant for this work are the sticking (γ) and accommodation coefficients (α). The accommodation coefficient ($0<\alpha\leqslant 1$) is the fraction of reflected atoms that undergo diffuse reflection on a wall, i.e., that have a postcollision velocity that is unrelated to the precollision velocity. For a fraction $1-\alpha$ of the reflected atoms, only the normal velocity component is reversed (specular reflection). The use of an accommodation coefficient is a first approximation of the physical phenomena that actually occur during surface interaction: normally, atoms are influenced partly by the interaction, i.e. their velocity changes but to some extent remains related to the original velocity. Since the silicon sidewalls of the trench and the membrane are smooth and clean, it is reasonable to assume values for accommodation coefficients below unity.[47]

Simulations for the y direction (see Figs. 4 and 6) were performed in a 2D simplification of the geometry (see Fig. 3), including the trench and the mask-to-substrate gap. The size of this gap, the sticking, and the accommodation coefficients were varied, whereas in each simulation identical values for γ and α were used on the mask and the membrane. The result of each simulation is a profile of the deposited metal film on the membrane. The height of the profile cannot be compared directly to the height of the experimental profile because the mass flux at the entrance of the trench is not known. However, due to the free-molecular nature of the

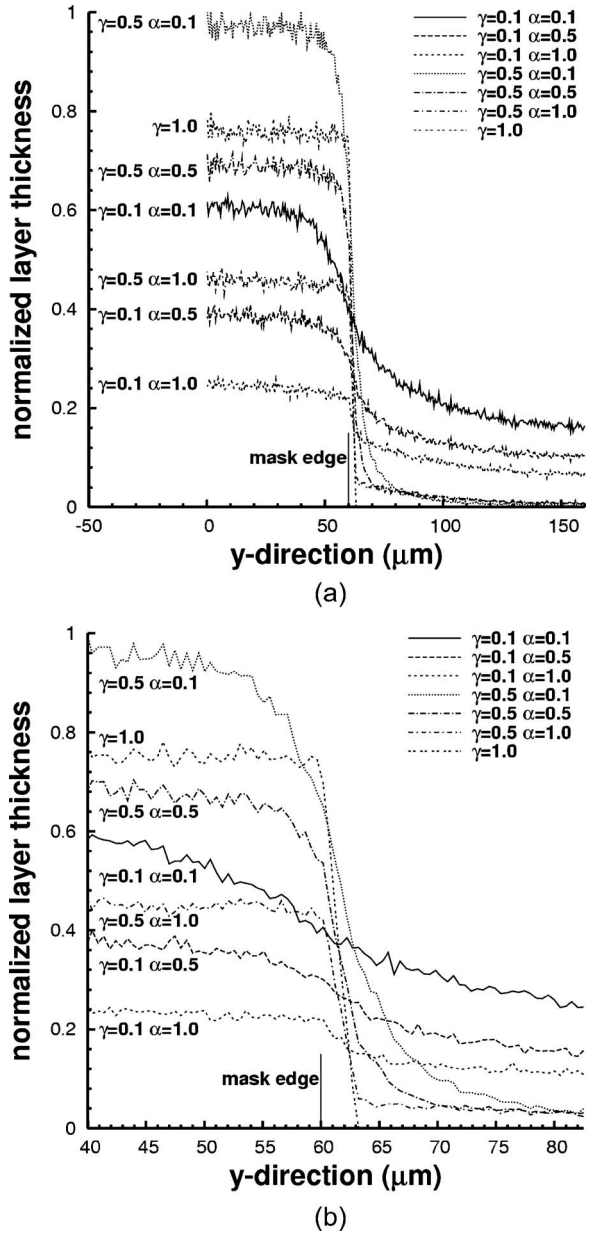

FIG. 9. Simulations of rhodium patches sputter-deposited through the shadow mask (gap of 25 μm) for different values of the sticking (γ) and accommodation coefficients (α)—(b) is a zoom in of (a).

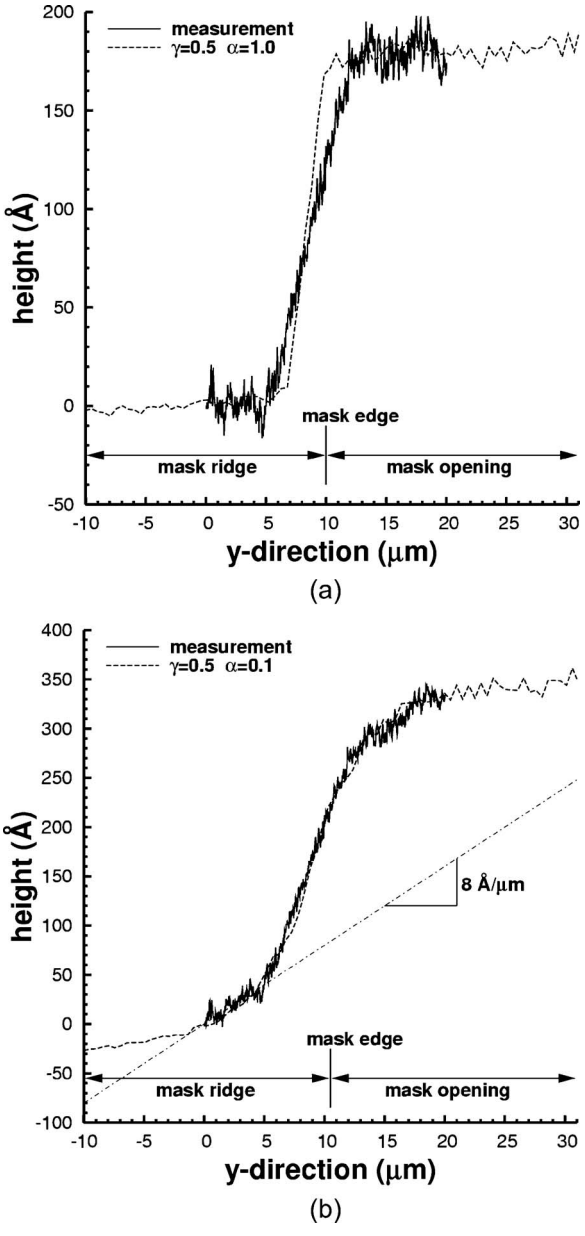

FIG. 10. Fitting of experimental and numerical data: poor agreement for $\gamma=0.5$ and $\alpha=1$ (a) and good agreement for $\gamma=0.5$ and $\alpha=0.1$ (b) [for both graphs similar experimental data is used, but for (b) this data were corrected with 8 Å/μm (see text)].

flow, the shape of the simulated profile can be compared directly to the experimentally observed profile after scaling.

In Fig. 9 simulated profiles of the metal pattern are shown for different values of γ (0.1, 0.5, and 1) and α (0.1, 0.5, and 1) for a gap of 25 μm, as obtained with the DSMC method. The layer thickness in the middle of the trench ($y=60$ μm) increases with increasing γ and/or decreasing α. Moreover, it is clear that for all cases with $\gamma<1$ metal is found on the membrane area outside the edge of the shadow mask: the lower the values of γ and α, the larger the pattern spreading. Furthermore, from the zoom in [Fig. 9(b)] near the edge of the trench it follows that for $\gamma<1$ the layer thickness already starts to decrease in the area covered by the mask (thus for $y<60$ μm). Simulations for $\gamma=0.1$ show a very gradual transition in the profile near the edge of the trench/ridge, whereas for $\gamma=0.5$ and $\alpha<1$ a more pronounced transition is observed. For $\gamma\geqslant 0.5$ and $\alpha=1$ there is an abrupt change in film thickness. Finally, for a sticking coefficient of unity the value of the accommodation coefficient is not relevant, since there is no reflection of atoms.

Based on these DSMC results and the pronounced but smooth transition measured in the layer thickness at the edge of catalyst patch [Fig. 7(a)], attention is focussed on simulations with $\gamma=0.5$ (Fig. 10). After scaling and adding of a dc offset to the simulated results (to match the origins of the measurement and simulation), it is found that the simulated pattern spreading for the case $\gamma=0.5$ and $\alpha=1$ is significantly

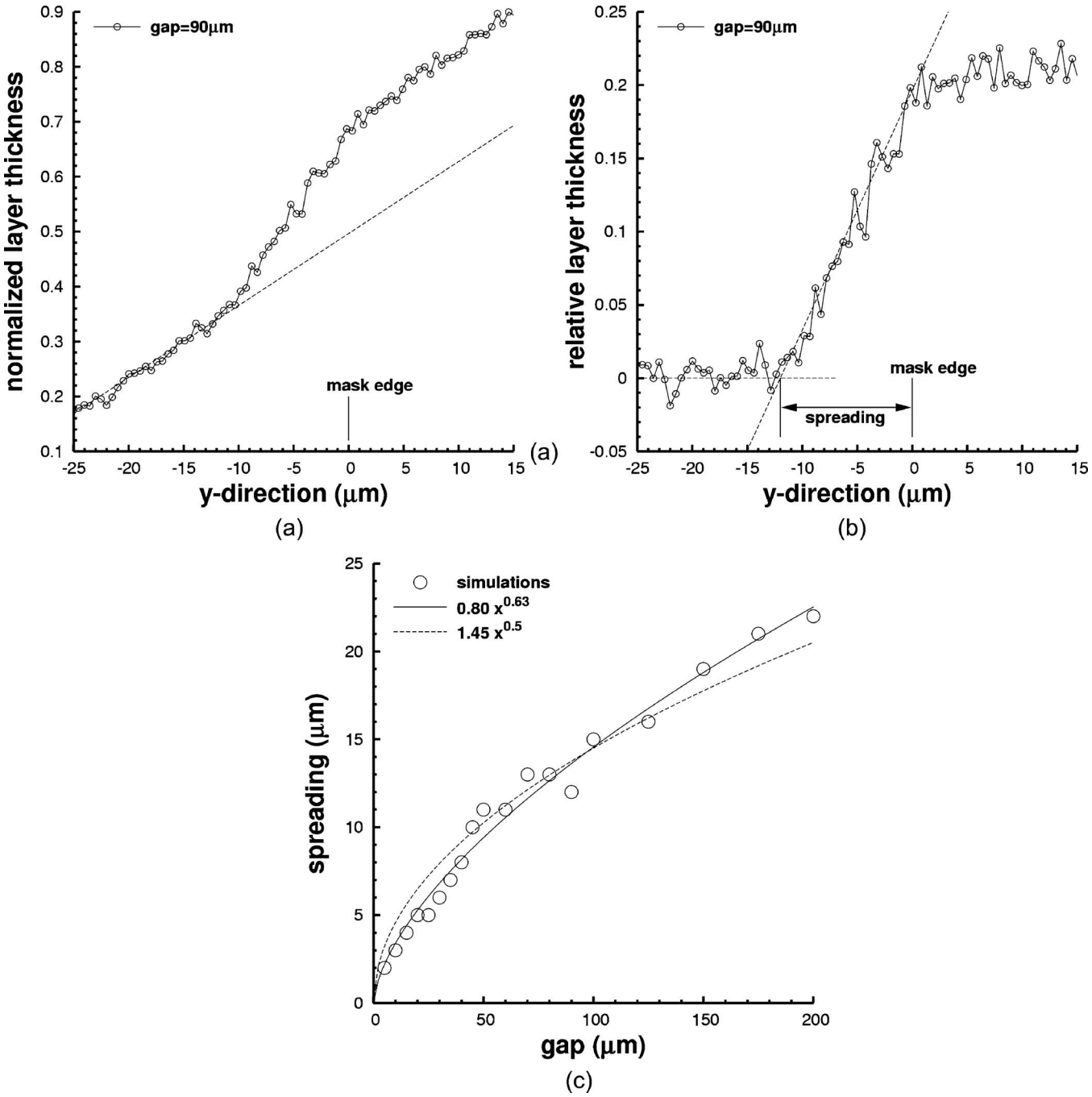

FIG. 11. Spreading of rhodium patches as a function of the gap as obtained from the DSMC model: uncorrected numerical data (for $\gamma=0.5$ and $\alpha=0.1$, gap=90 μm)—dotted line indicates baseline correction level (a); corrected numerical data (for $\gamma=0.5$ and $\alpha=0.1$, gap=90 μm)—dotted lines used to localize spreading (b); spreading of rhodium patches as a function of mask-to-substrate gap (c).

smaller than the measured spreading [Fig. 10(a)]. Simulations performed with $\gamma=0.5$ and $\alpha=0.1$ lead to a pattern spreading in close agreement with experimental data. However, as shown in Fig. 10(b), these simulations show that deposition takes place much further outside the mask edge than was assumed in the experiments. Therefore, the lowest experimentally observed film thickness (at $y=0$ μm) most probably does not correspond to a zero film thickness, and the slope of the thickness profile at this location is not zero. To correct for this effect, the initially measured film thickness profile as a function of y was recalculated with respect to a baseline with a slope of 8 Å per μm [indicated as a dashed line in Fig. 10(b)], Here, this correction led to a perfect agreement between experiments and simulations, justifying this procedure. It can thus be concluded that the length of the selected area of the experimental profile was too short to observe the real baseline on which levelling could be based. A factor of 8 Å/μm is reasonable for this configuration, since the silicon, in which the shadow mask is etched, as well as the substrate, both have a curvature of 10 μm, and

one (or both) might deflect slightly during catalyst deposition. Due to good agreement between the DSMC model and the experimental data for a gap of 25 μm (using $\gamma=0.5$, $\alpha=0.1$, and applying a baseline correction), these settings are used for further simulations in which the pattern spreading is studied as a function of the size of the gap between shadow mask and membrane. As described above, a baseline shift was applied to all simulations in order to compare them to the experimental data.

In Fig. 11 this procedure is shown, as well as the spreading as a function of the gap as modeled with the DSMC method. Figure 11(a) shows the uncorrected simulation ($\gamma=0.5$, $\alpha=0.1$) for a gap of 90 μm. The dotted line indicates the baseline that is used to transform this data to the curve of Fig. 11(b). This baseline is selected such that in the corrected numerical data a transition zone can be clearly distinguished, and that the profile on both sides of the transition zone is more or less flat. With the latter plot [Fig. 11(b)] the spreading in the deposited pattern can be determined as the distance between the mask edge and the outer edge of the transition. This procedure is performed for gaps in the range of 5–200 μm (for each gap a different baseline was used), and the resulting values for the spreading in the metal patches are shown in Fig. 11(c). Although the best fit is a relation in which the spreading scales with the gap to the power 0.63, a square root relation yields a reasonable fit as well [Fig. 11(c)].

Clearly, the modeled spreading as a function of the gap size matches well with the experimental data (Fig. 8), in terms of the trend as well as the actual values. It is noted that the small differences in spreading values between the experimental data and the simulation model [Figs. 8 and 11(c)] could be due to imperfections of the method to measure the spreading, as well as the baseline correction procedure of the numerical data. Since an optical method is used, it is difficult to observe ultrathin metal layers (<2 nm), which introduces small errors in the measured spreading of the patches. Another reason is the determination of the slope of the baseline. Since this is done manually [in order to obtain a profile that has flat zones on both sides of the transition zone—Fig. 11(a) and 11(b)], especially at large(r) gaps, an uncertainty arises in the spreading values. Nevertheless, the good agreement between modeled data and experimental results for the shape of the metal patches deposited through the shadow mask and the spreading of this patch (both in the y direction) proves that the used DSMC model with the assumptions for the sticking and accommodations coefficients ($\gamma=0.5$, $\alpha=0.1$) is a good model to estimate (and control) the spreading of catalytic patches deposited onto a membrane located at the bottom of a deep, rectangular trench. The spreading in the x direction (parallel to the alignment ridges) is not modeled, since this requires a time-consuming 3D model. However, since there is a good agreement between the 2D DSMC model and experimental data for the y direction (perpendicular to ridges), it is assumed that the experimental pattern spreading in the x direction (which was rather difficult to determine experimentally for gaps larger than 25 μm) can be explained as well with values for the sticking and accommodation coefficients below unity (i.e., $\gamma=0.5$, $\alpha=0.1$) and curvature and/or bending of the shadow mask, substrate, and/or membrane.

V. CONCLUSIONS

In this work the application of a 3D self-aligning shadow mask in (110)-oriented silicon is discussed. This shadow mask can be used for the deposition of metal tracks on the bottom of structures with vertical sidewalls, i.e., patterning of rhodium catalytic patches underneath the membrane that covers the deep flow channel of a high-temperature gas microreactor. The accuracy of this patch definition—pattern spreading—is investigated for different metals and as a function of the mask-to-substrate distance.

The pattern of sputter-deposited patches is subject to pattern spreading when the gap between the shadow mask and the substrate is nonzero. The experimental patch widening shows a square root dependency on the gap size. Via numerical simulations of molecular gas flows (using a direct simulation Monte Carlo method), it is shown that this relation between spreading and mask-to-substrate distance can be explained by assuming that both the sticking (γ) and accommodation (α) coefficients of the atoms on the walls are significantly lower than unity. Excellent agreement between the experiments and model is found for $\gamma=0.5$ and $\alpha=0.1$ after correcting for the curvature or bending of the shadow mask and/or substrate.

ACKNOWLEDGMENTS

This work was supported by the Dutch Technology Foundation (STW—project "FORSiM," No. EFC.5134) and by the Netherlands Organization for Applied Scientific Research (TNO). J.W. Mertens is thanked for his assistance in the clean room activities.

[1] A. Mehra, X. Zhang, A. A. Ayón, I. A. Waitz, and M. A. Schmidt, J. Vac. Sci. Technol. B **18**, 2583 (2000).
[2] R. Srinivasan *et al.*, AIChE J. **43**, 3059 (1997).
[3] T. Becker, S. Mühlberger, C. Bosch-v. Braunmühl, G. Müller, A. Meckes, and W. Benecke, J. Microelectromech. Syst. **9**, 478 (2000).
[4] V. G. Kutchoukov, J. R. Mollinger, M. Shikida, and A. Bossche, Sens. Actuators, A **A92**, 208 (2001).
[5] N. P. Pham, E. Boellaard, J. N. Burghartz, and P. M. Sarro, J. Microelectromech. Syst. **13**, 491 (2004).
[6] V. K. Singh, M. Sasaki, J. H. Song, and K. Hane, Jpn. J. Appl. Phys., Part 1 **44**, 2016 (2005).
[7] P. Kersten, S. Bouwstra, and J. W. Petersen, Sens. Actuators, A **A51**, 51 (1995).
[8] C. Christensen, P. Kersten, S. Henke, and S. Bouwstra, IEEE Trans. Compon., Packag. Manuf. Technol., Part A **19**, 516 (1996).
[9] M. Heschel and S. Bouwstra, Sens. Actuators, A **A70**, 75 (1998).
[10] L. S. Johansen, M. Ginnerup, J. T. Ravnkilde, P. T. Tang, and B. Löchel, Sens. Actuators, A **A83**, 156 (2000).
[11] R. Schnupp, R. Baumgärtner, R. Kühnhold, and H. Ryssel, Sens. Actuators, A **A85**, 310 (2000).
[12] V. G. Kutchoukov, J. R. Mollinger, and A. Bossche, Sens. Actuators, A **A85**, 377 (2000).
[13] L. I. Maissel, R. Glang, and L. V. Gregor, in *Handbook of Thin-Film Technology*, edited by R. Glang (McGraw-Hill, New York, 1970), Vol. 1, Chap. 7, p. 1.
[14] P. F. Tian, V. Bulovic, P. E. Burrows, G. Gu, S. R. Forrest, and T. X.

Zhou, J. Vac. Sci. Technol. A **17**, 2975 (1999).
[15]R. Dizon, H. Han, A. G. Russell, and M. L. Reed, J. Microelectromech. Syst. **2**, 151 (1993).
[16]H. Sheng, D. Fujita, T. Ohgi, H. Okamoto, and H. Nejoh, Mod. Phys. Lett. B **12**, 597 (1998).
[17]K. Ono, H. Shimada, S. Kobayashi, and Y. Ootuka, Jpn. J. Appl. Phys., Part 1 **35**, 2369 (1996).
[18]J. Kohler, M. Albrecht, C. R. Musil, and E. Bucher, Physica E (Amsterdam) **4**, 196 (1999).
[19]R. Lüthi, R. R. Schlitter, J. Brugger, P. Vettiger, M. E. Welland, and J. K. Gimzewski, Appl. Phys. Lett. **75**, 1314 (1999).
[20]J. Brugger, J. W. Berenschot, S. Kuiper, W. Nijdam, B. Otter, and M. Elwenspoek, Microelectron. Eng. **53**, 403 (2000).
[21]M. Kölbel, R. W. Tjerkstra, J. Brugger, C. J. M. van Rijn, W. Nijdam, J. Huskens, and D. N. Reinhoudt, Nano Lett. **2**, 1339 (2002).
[22]G. M. Kim, M. A. F. van den Boogaart, and J. Brugger, Microelectron. Eng. **67–68**, 609 (2003).
[23]T. Schallenberg, T. Borzenko, G. Schmidt, L. W. Molenkamp, S. Rodt, R. Heitz, D. Bimberg, and G. Karczewski, J. Appl. Phys. **95**, 311 (2004).
[24]M. M. Deshmukh, D. C. Ralph, M. Thomas, and J. Silcox, Appl. Phys. Lett. **75**, 1631 (1999).
[25]C. V. Cojocaru, C. Harnagea, F. Rosei, A. Pignolet, M. A. F. van den Boogaart, and J. Brugger, Appl. Phys. Lett. **86**, 183107 (2005).
[26]H. J. Shin, J. H. Choi, H. J. Yang, Y. D. Park, Y. Kuk, and C. J. Kang, Appl. Phys. Lett. **87**, 113114 (2005).
[27]M. A. F. van den Boogaart, M. Lishchynska, L. M. Doeswijk, J. C. Greer, and J. Brugger, Sens. Actuators, A **A130–A131**, 669 (2006).
[28]G. J. Burger, E. J. T. Smulders, J. W. Berenschot, T. S. J. Lammerink, J. H. J. Fluitman, and S. Imai, Sens. Actuators, A **A54**, 669 (1996).
[29]S. Gray and P. K. Weimer, RCA Rev. **20**, 413 (1959).
[30]J. Brugger, C. Andreoli, M. Despont, U. Drechsler, H. Rothuizen, and P. Vettiger, Sens. Actuators, A **A76**, 329 (1999).
[31]S. B. Schaevitz, A. J. Franz, K. F. Jensen, and M. A. Schmidt, *Proceedings of the 11th International Conference on Solid-State Sensors and Actuators (Transducers 2001)*, Munich, Germany, June 10–14 (Springer, Berlin, 2001), p. 30.
[32]C. R. H. de Smet, Ph.D. thesis, Eindhoven University of Technology, 2000.
[33]D. A. Hickman, E. A. Haupfear, and L. D. Schmidt, Catal. Lett. **17**, 223 (1993).
[34]R. M. Tiggelaar *et al.*, Sens. Actuators, A **A112**, 267 (2004).
[35]R. M. Tiggelaar *et al.*, Sens. Actuators, A **119**, 196 (2005).
[36]L. D. Kendall, Annu. Rev. Mater. Sci. **9**, 373 (1979).
[37]J. G. E. Gardeniers, H. A. C. Tilmans, and C. C. G. Visser, J. Vac. Sci. Technol. A **14**, 2879 (1996).
[38]M. Vangbo and Y. Bäcklund, J. Micromech. Microeng. **6**, 279 (1996).
[39]L. T. Ball, I. S. Falconer, D. R. McKenzie, and J. M. Smelt, J. Appl. Phys. **59**, 720 (1986).
[40]G. M. Turner, I. S. Falconer, B. W. James, and D. R. McKenzie, J. Appl. Phys. **65**, 3671 (1989).
[41]W. D. Westwood, J. Vac. Sci. Technol. **15**, 1 (1978).
[42]S. D. Ekpe and S. K. Dew, J. Vac. Sci. Technol. A **21**, 476 (2003).
[43]J. A. Thornton, Thin Solid Films **54**, 23 (1978).
[44]J. A. Thornton and J. L. Lamb, Thin Solid Films **119**, 87 (1984).
[45]H. Kersten, G. M. W. Kroesen, and R. Hippler, Thin Solid Films **332**, 282 (1998).
[46]T. P. Drüsedau, T. Bock, T.-M. John, F. Klabunde, and W. Eckstein, J. Vac. Sci. Technol. A **17**, 2896 (1999).
[47]H. Steffen, H. Kersten, and H. Wulff, J. Vac. Sci. Technol. A **12**, 2780 (1994).
[48]G. A. Bird, *Molecular Gas Dynamics and the Direct Simulations of Gas Flows*, Oxford Engineering Science Series nr. 42 (Clarendon, Oxford, 1994).
[49]R. Dorsman and C. R. Kleijn, *Proceedings of the Chemical Vapor Deposition XCI and EUROCVD-14 (CVD XVI & EUROCVD-14)*, Paris, France, April 27–May 2, 2003 (Electrochemical Society, New York, 2003), Vol. 2003-8, p. 171.
[50]R. Dorsman, AIP Conf. Proc. (to be published).
[51]R. Dorsman, C. R. Kleijn, J. Velthuis, J. P. Zijp, and A. van Mol, J. Vac. Sci. Technol. A **25**, 474 (2007).